Proposal for a Scintillator Tile Hodoscope for $\overline{\mathsf{P}}$ANDA

Version 1.1

K. Goetzen, H. Orth, G. Schepers, L. Schmitt, C. Schwarz

Abstract

In this document a new detector in place of the barrel time-of-flight detector is proposed. This detector is based on small scintillator tiles read out by silicon photomultipliers. The motivation in terms of physics and technical benefits are summarized. Details of the detector layout are given.

Contents

1 Introduction

In this document a new detector in place of the barrel time-of-flight detector is proposed. The main criticism of previous concepts of barrel time-of-flight detectors is the material budget deteriorating the performance of the lead tungstate crystal calorimeter. In addition the available space in radial direction is extremely tight so that some detector concepts have problems to fit in. The concept presented here takes the optimization of material and thickness to the extreme implementing a timing detector with less than 2% of a radiation length and less than 2 cm radial thickness including readout and mechanics. This detector is based on small scintillator tiles read out by silicon photomultipliers. A time resolution of better than 100 ps should be achieved by the system to allow for good time-of-flight measurement and other timing applications. Apart from physics applications requiring time-of-flight measurements in the barrel region several technical benefits are important to consider, most notably the usage for software triggering and event building purposes.

In the first sections the motivation in terms of physics and technical benefits are summarized. In the following section details of the detector layout are given. Finally first considerations concerning the project organization are given. The start of the project depends on a positive decision on the concept by the $\overline{\mathsf{P}}$ANDA collaboration.

2 Physics Motivation

2.1 Hypernuclear Physics

Hypernuclear research will be one of the main topics addressed by the $\overline{\mathsf{P}}$ANDA experiment [1] at FAIR [9]. The $\overline{\mathsf{P}}$ANDA hypernuclear programme will reveal the strength of Λ–Λ interaction via high resolution γ spectroscopy of double Λ hypernuclei. In contrary to past hypernuclear experiments, where only a few double hypernuclei events were found, the challenge of the $\overline{\mathsf{P}}$ANDA experiment will be to increase statistics by five orders of magnitude. Germanium detectors, despite their good energy resolution, have an efficiency of only a few percent.

In combination with the high luminosity of the antiproton beam at HESR, a high production rate of single and double hypernuclei under unique experimental conditions will be possible for the first time.

In the $\overline{\mathsf{P}}$ANDA experiment, double hypernuclei will be produced as a result of a multi–stage process. In the first stage a Ξ^- (together with its associated strange particle) is produced in a primary target via the reaction $\overline{p} + p \rightarrow \Xi^-\overline{\Xi}^+$. The $\overline{\Xi}$ will undergo scattering or (in most cases) annihilation inside the residual nucleus. Strangeness is conserved in the strong interaction and the annihilation products contain at least two anti-kaons that can be used as a tag for the reaction.

In a second stage, the Ξ^- is slowed down in a dense, solid material (e.g. a nuclear emulsion) and forms a Ξ^- atom [6]. After an atomic cascade, the hyperon is finally captured by a secondary target nucleus. If the momentum of the hyperon is too high its stopping time will exceed the lifetime and hence the Ξ^- will decay prior to the atomic capture with high probability. In order to

reach a high capture probability it is mandatory to keep the primary momentum of the produced Ξ^- as low as possible.

The energy release of about 28 MeV during the conversion of the Ξ^- into two Λ hyperons may give rise to the emission of particles from the nucleus (*double* Λ *compound nucleus*), where the conversion took place. As a consequence, a variety of double, single or twin hypernuclei as well as ordinary nuclei may be produced in excited states.

The hypernuclei study will make use of the modular structure of the $\overline{\mathsf{P}}$ANDA detector. Removing the backward end-cap calorimeter will allow to add a dedicated nuclear target station and the required additional detectors for γ spectroscopy close to the entrance of $\overline{\mathsf{P}}$ANDA.

The major difficulty to accomplish this project resides in the complexity of the hypernuclei production mechanism and in the identification procedure. Furthemore, the $\bar{p}p \rightarrow \Xi^-\overline{\Xi}$ cross section of 2μb is about a factor 25000 smaller than the total $p\bar{p}$ cross section of 50 mb at 3 GeV/c.Therefore an efficient background suppression is mandatory. As it was remarked before, the associated anti-hyperon annihilates with large probability ($\simeq 85\%$ [1]) within the primary target nucleus releasing at least two positive kaons which can be used to tag the hypernuclei production. Kaons produced in this way are emitted in the forward direction (beam direction) and with a momentum distribution around 500 MeV/c. Here the difficulty resides in finding a proper detector system to identify efficiently positive kaons.

In the current $\overline{\mathsf{P}}$ANDA design, particle identification for slow particles (below 700 MeV/c) may be provided at large polar angles by a Time Of Flight (SciTil) detector in combination with the central tracker. This issue is the topic of a different report [2] and can be summarized as follows: The associated $\Xi\ \overline{\Xi}$ production allows to trigger on the $\overline{\Xi}$ to suppress the background by many orders of magnitude. For the planned ^{12}C primary target 15% of the $\overline{\Xi}$ leave the target and decay. The other 85% annihilate within the target and produce due to strangeness conservation two kaons. The number of positive charged kaons produced in this process amounts to approximately 40%. Here, the reconstruction probability of the kaons is about 28%. These results are the predictions from a URQMD+SMM model [8] containing the production of $\Xi\ \overline{\Xi}$ and the partial annihilation of the $\overline{\Xi}$. The background contribution to the kaon trigger amounts to 7.7% and is modeled by the URQMD model [7] not containing the above mentioned processes. Triggering on the positive kaons increases the total trigger rate by a factor of 7. The barrel DIRC can measure 55% of these kaons while 45% are below its momentum threshold. The benefit of a positive kaon identification below the momentum threshold of the barrel DIRC is a factor of 2 higher trigger rate.

2.2 Conclusions from the TAG PID

In the report of the Technical Assessment Group on Particle Identification (TAG PID) [3] to the $\bar{\mathsf{P}}$ANDA collaboration all informations to the PID sub-detectors planned at that time are collected as well as a method is introduced to define and evaluate the performance of detector parts and a complete detection system for a positive particle identification.

As one of the PID detectors a Barrel-Time-of-Flight detector was evaluated in combination with the two options of the central tracker for the target spectrometer being a STT or a TPC. No

[1] Probability is given by the UrQMD model

Endcap-ToF was considered in this report. The Barrel-ToF detectors proposed were two types of RPCs and a ToF scintillator barrel covering the polar angles Θ from 22° to 140°. Their position was allocated inside the Barrel-DIRC radius. As simulated by the working groups behind these different types all solutions for the Barrel-ToF provide a valuable pion-Kaon separation below the Cherenkov-threshold and a Kaon-proton separation up to 1.5 GeV/c.

Since at the time of the preparation of the report no full simulation was available a fast simulation was introduced [3] using the parameterization of the different PID processes. All known specific detector effects were input for this simulation package.

With this tool the separation power, defined in the report, could be determined for each combination of two different particle species. The separation power was calculated for a fine binning of the solid angle θ covered (by each sub-detector) and the momentum p of the produced particles.

The combination of all detectors results in a map of separation power over θ and p. In regions (bins) covered by more than one detector the global separation power was calculated as the quadratic sum of the separation power of the contributing detectors. Due to its higher sensitivity to small differences the separation power has been translated into the so called mis-identification level for the process of evaluation and comparison.

The connection to the envisaged physics is achieved by comparing phase space plots over θ and p with the map of separation power, whereas the only interesting regions are those where the signal overlaps with the background particles. For all $\bar{\text{P}}$ANDA relevant physics channels and its relevant background channels phase space plots were produced and the overlap regions were determined. Only for these regions the average fraction of mis-identification was determined.

For all four scenarios of the detector setup, i.e. with the STT, the STT plus a Barrel-ToF, the TPC and the TPC plus a Barrel-ToF, a factor relative to the above value has been computed. These numbers allow to evaluate the performance of the four options.

In the fast simulation a start detector was assumed having with δt=100 ps the same uncertainty in the time measurement as the Barrel-ToF detector. This lead to an over-all time resolution for the ToF of 141 ps. (Running without a start detector improves the time resolution but this requires to run the ToF with a relative timing.)

As emphasized with three examples identified (and shown in dedicated plots) in the report [3] the Barrel Time of Flight detector can add in some cases beneficial positive PID information to the case where otherwise only dE/dx from the central tracker (the STT or the TPC) is available:

- $\bar{p}p \rightarrow D^0\bar{D}^0\gamma$ at 6.488 GeV/c (K/p) and $\bar{p}p \rightarrow \Lambda^0\bar{\Lambda}^0$ at 10 GeV/c (p/K) These channels are good examples for scenarios where the Barrel TOF system can add valuable information for the purpose of proton-Kaon separation. In particular with the STT as the central tracker the mis-ID decreases by a factor of approximately eight. In case of the TPC option this improvement is reduced since the dE/dx information can be expected to provide sufficiently powerful information for good identification.

- $\bar{p}p \rightarrow \Lambda_c^+\Lambda_c^-$ at 10.187 GeV/c (π/K) The pions originating form this baryonic channel cover a large part of the relevant phase space for π/K separation. The critical region is the low momentum edge of the distributions below 400 MeV/c. Here it can be seen, that in case

of the STT tracker option a Barrel TOF significantly improves the identification power. Obviously in this particular situation the dE/dx information of the TPC alone already provides better identification potential than the combined information of STT and TOF. These cases can be seen as example for all charmed baryons.

The information for these three channels extracted from the TAG PID report are summarized in table 1. For the four different detector setups described above the momentum of the antiproton beam $p_{\bar{p}}$, the signal channel, the particular particle species of signal and background, the minimum average separation power of the four setups, the maximum average mis-identification level $f_{mis,max}$ and the relative ratio $f_{mis,i}/f_{mis,max}$ are listed in blue. Thus the worst identification capability of a detector setup is the value 1.0 for this ratio, all smaller values denote a solution supperior to this.

$p_{\bar{p}}$ [GeV/c]	Signal	PID	min σ	mis[%]	STT	STT+TOF	TPC	TPC+TOF
6.488	$D^0\bar{D}^0\gamma$	π - K	6.0	0.1	1.0	0.2	0.1	0.0
		π - p	4.8	0.8	1.0	0.2	0.4	0.3
		K - π	5.4	0.3	1.0	0.2	0.2	0.1
		K - p •	4.8	0.8	1.0	0.1	0.1	0.1
10.000	$\Lambda^0\bar{\Lambda}^0$	π - K	3.8	2.7	1.0	1.0	0.7	0.7
		π - p	3.4	4.6	1.0	1.0	0.7	0.7
		p - π	5.5	0.3	1.0	0.1	0.1	0.1
		p - K •	5.4	0.4	1.0	0.1	0.1	0.0
10.187	$\Lambda_c^+\Lambda_c^-$	π - K	4.3	1.5	1.0	0.9	0.6	0.6
		π - p	3.6	3.7	1.0	0.9	0.7	0.8
		K - π	4.5	1.2	1.0	1.0	0.8	0.8
		K - p	3.4	4.6	1.0	0.9	0.7	0.7
		p - π	3.5	4.1	1.0	0.9	0.9	0.8
		p - K	3.5	4.1	1.0	1.0	0.8	0.8
		π - K •	4.3	1.7	1.0	0.8	0.6	0.6
		K - π	4.5	1.2	1.0	1.0	0.8	0.8
		p - π	3.5	4.0	1.0	1.0	0.8	0.9
		p - K	3.5	4.1	1.0	0.9	0.8	0.8

Table 1: Influence of a Barrel-ToF detector on the mis-identification value of two particle species. The commented examples are marked with a point.

Since no Endcap-Time-of-Flight detector as it is now proposed with the Forward-Endcap SciTil was evaluated by the PID-TAG an addition to the conclusions of the report may be allowed and an example might be given where the influence of this proposed detector becomes clear:

$\bar{p}p \rightarrow D^0\bar{D}^0\gamma$ at 15 GeV/c (K/p)

As visible in the map of separation power/misidentification ([3], Fig.62) a Time-of-Flight measurement of the Kaons and protons ejected in the forward region between 10° to 22° with momenta below 1.5 GeV/c could close the existing gap of insufficient separation of the two particle species.

It has to be noted again that the report and its conclusions are based on a fast simulation. This means that for the results no microscopic simulation was done. The PID processes were parameterized and some estimations were done for simplification or since no better knowledge was available. Nevertheless the positive influence of a Time-of-Flight measurement in the Target-Spectrometer to the charged particle identification in $\bar{\text{P}}$ANDA -first of all below the relevant Cherenkov threshold - is obvious. The SciTil solution proposed here corresponds to a reduced material amount, a larger flight length from the interaction point, a closer distance to the Electromagnetic Calorimeter and a larger solid angle coverage compared to the solutions evaluated in the report. All these advantages lead to a further improvement in the performance of the Time-of-Flight system.

2.3 First Physics

PANDA has no hardware trigger but continuously digitizes all detector signals after autonomous hit-detection. Once the data of one time frame of approx. 500 μs (*super burst*) is assembled the processing for the event selection can start. The complete processing of all events at the full interaction rate is not possible since this would require computing resources exceeding the cost of the entire experiment. This holds even for the beginning when data taking will still run at a factor of 10-100 lower rate. Therefore simple signatures have to be used for a *software trigger*, i.e. a very fast first selection level which takes only few microseconds. Depending on the available computing power a reduction of 100-1000 has to be achieved in the first fast selection.

The first step in the event selection is called software trigger. This trigger is based on a simple algorithm based on one or few detectors. It does not require long computational operations but is based on correlations of digital signals. The goal is to achieve high rejection factors from simple signatures. More refined processing takes place at higher levels. Typical examples for software triggers are very much in analogy to their familiar hardware ancestors and cut on particle multiplicity, particle coincidences in time, or simple track pointing.

In the beginning of the experimental life of $\overline{\text{P}}$ANDA the complex detector systems like electromagnetic calorimeter, central tracker and micro vertex detector have to be calibrated and aligned carefully and details of their stable operation have to be established in practice. In such a phase these detectors are not suited at all as input for the fast software trigger: Any signature based on not understood or simply not well calibrated detectors will be spurious and unreliable and create a biased signature. Drawing physics observations from these signatures will be difficult or even erroneous. Like at the beginning of any simple test experiment it is therefore necessary to base the input for further better understanding of a complex detector system on simple and reliable scintillators for reference.

The system presented in this proposal will allow exactly this simple approach for a deeper understanding of the other more complex systems. At the same time it provides with its high granularity and time resolution a very robust tool for software triggers in the first physics run. This will not yet comprise the selection of very complex channels from the list of $\overline{\text{P}}$ANDA highlights but it will allow to establish a relation to previous measurements and publish first physics results rather quickly.

In case of absence of the SciTil detector at the very beginning the risk is that no physics topics

can be addressed for a longer period of time. For an expensive and complex experiment like $\overline{\mathsf{P}}$ANDA this would be a very bad start. Other hadron and particle physics experiments were in this situation and failed at least partially. The experiments at LHC have learned this lesson and successfully prepared for first physics based on simple signatures.

3 Technical Motivation

3.1 Event Timing

In addition to the contribution of a time-of-flight detector system leading to an increased performance of particle identification, a high time resolution will serve as an essential ingredient for any event building algorithm. This issue has been intensively studied, and the detailed results can be found in [4].

One of the key features of the PANDA experiment will be a high luminosity mode with sufficiently high event rates to tackle physical questions with adequate statistical power. In this mode the average event rate given by the product of the average luminosity of $\mathcal{L} = 2 \cdot 10^{32}$ cm^{2}s$^-$1 and the total cross section $\sigma_{tot} \approx 100$ mb of $\bar{p}p$ scattering will be of the order of $\dot{N}_{\mathrm{avg}} = 20$ MHz.

Since the luminosity is a time dependent quantity influenced by both the beam current in the HESR as well as the spatial distribution of the target[2], significant higher instantaneous[3] event rates up to $\dot{N}_{\mathrm{max}} = 100$ MHz have to be taken into account. The average time difference between two events in that case is given by already challenging $\delta t_{\mathrm{avg}} = 1/\dot{N}_{\mathrm{avg}} = 10$ ns, i. e. on that time scale all detector signals have to be collected to form event data packages. This technical challenge finally is intensified by the fact that the events are not distributed equidistant in time but exhibit an exponential behaviour concerning the time difference between sequent events as illustrated in Fig. 1.

This means that smaller time differences are in general more likely; in fact the probability density function has a maximum at $\delta t = 0$ ns. In particular 63% of all reactions have a δt smaller than the average value. At this point it seems clear that a high resolution timing is desirable to disentangle signals from different events. In order to quantify the impact of time resolution to the event building performance the basic concept of event selection will be defined in the following.

An event takes place at a certain time t_0. The particles originating from that reaction will travel for some time with a certain velocity before they hit a timing detector. Each particle i creates a signal at wall clock time t_i. Under the assumption that momentum measurements and particle identification is available at least on an approximate level, the velocity v and trajectory length s can be determined. Together with the time measurement t_i the time of origin $\mathrm{t}_{0,i} = t_i - s/v$ can be computed[4]. If all the uncertainties are Gaussian these values should be distributed around the

[2]For the pellet target the current rate vanishes in times where no pellet is in the beam, leading to an additional factor between average and peak rate of about $\geq$2.

[3]The term *instantaneous* expresses the rate $\dot{N}(t')$ at a certain time t' in contrast to the average rate $\dot{N}_{\mathrm{avg}} = \frac{1}{\Delta t} \cdot \int_{t_0}^{t_0+\Delta t} \dot{N}(t)\, dt$ for large Δt.

[4]In particular for slow tracks particle identification is important to determine the velocity. For high momentum particles the approximation $\beta = 1$ leads to sufficiently good results.

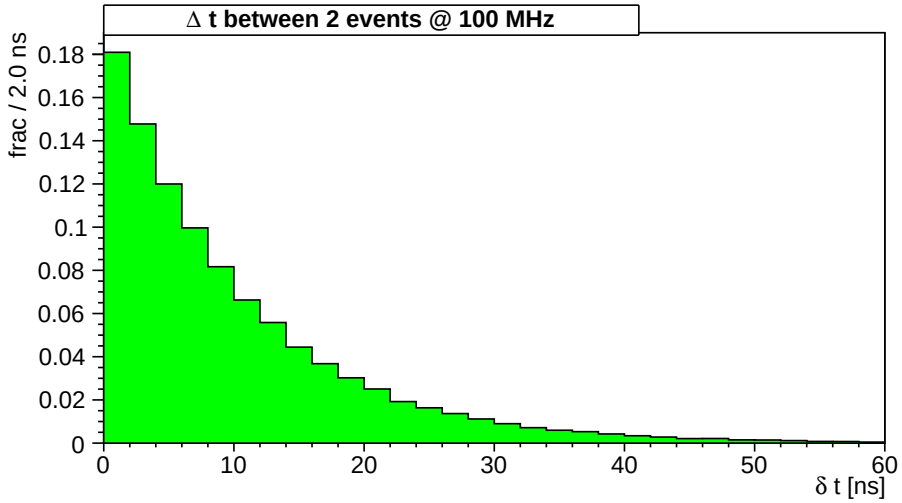

Figure 1: Distribution of the time difference δt between two sequent reactions at an instantaneous event rate of $\dot{N} = 100$ MHz.

event time t_0 with a total time resolution σ_t. Given a sufficiently good momentum resolution the value σ_t will be dominated by the time uncertainty of the best timing device.

In this approach the performance of event building depends on the spread of the $t_{0,i}$ distribution, i. e. the better the $t_{0,i}$ clusters of different reactions are separated in time, the higher the selection efficiency will be. Overlapping distributions however will result in efficiency loss, since these events cannot be separated anymore in a simple way. This is illustrated in fig. 2, where the clustering is shown for the two different time resolutions. The time signals of different events are colored cyclically with the colors black, red and blue. While in the first case with time resolution $\sigma_t = 0.1$ ns different events can be separated well, this feature gets partially lost in the second case with $\sigma_t = 2.0$ ns. The efficiency (non-overlap fraction) in that respect is defined as the fraction of events whose creation time distributions do not overlap with those of earlier or later ones.

The efficiency has been determined for reactions with 6 charged tracks as a function of the instantaneous rate in the range between 10 MHz and 100 MHz for four different time resolution values $\sigma_t \in \{0.1, 1.0, 2.0, 5.0\}$ ns. This choice intends to represent typical values for time-of-flight systems (100 ps), the range of the time resolution the electromagnetic calorimeter is able to deliver for charged tracks and in particular hadrons in PANDA (1 – 2 ns), and single hit performance of tracking detectors (5 ns). The four curves, colored in black, red, blue and magenta, respectively, are shown in fig. 3 (a).

Clearly visible is the superior efficiency for the best time resolutions of $\sigma_t = 0.1$ ns, which is the projected performance for the SciTil detector. Where the latter would allow the separation of the event time clusters up to 100 MHz with efficiencies of more than 95%, the corresponding values for $\sigma_t > 1$ ns are between roughly 60% ($\sigma_t = 1$ ns) and less than 10% ($\sigma_t = 5$ ns).

The values of pure non-overlap fractions are not necessarily equivalent to the efficiencies which could be achieved with a concrete algorithm. Therefore a very simple and straight-forward procedure for event selection has been applied to estimate a more realistic performance. The approach bases on the idea to consider all sequences of $t_{0,i}$ as event candidates which are separated by time

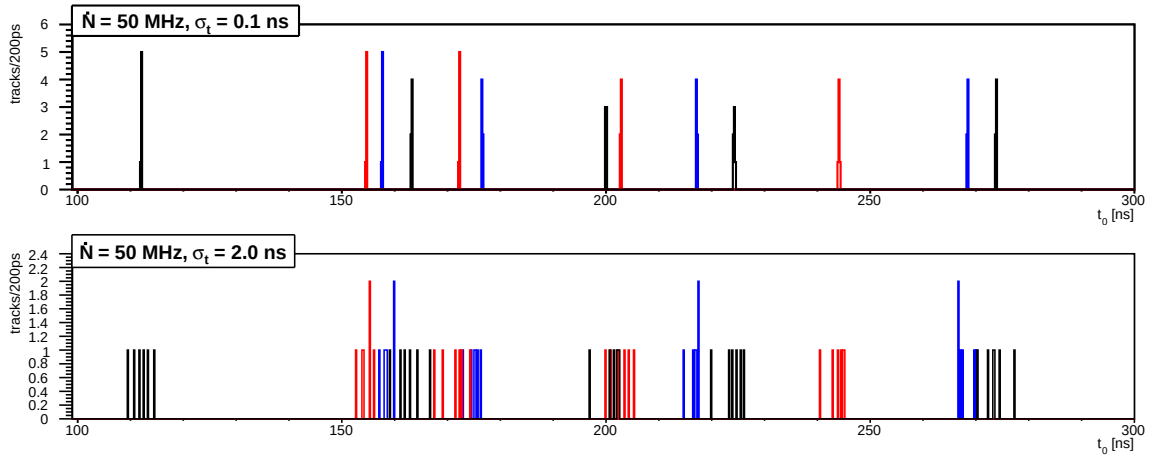

Figure 2: Illustration of $t_{0,i}$ distribution of reactions with 6 tracks at an instantaneous rate of $\dot{N} = 50$ MHz and total time resolutions of $\sigma_{t1} = 100$ ps (top) and $\sigma_{t2} = 2$ ns (bottom). The three color black, red, and blue are cyclically used to mark time signals $t_{0,i}$ from different events.

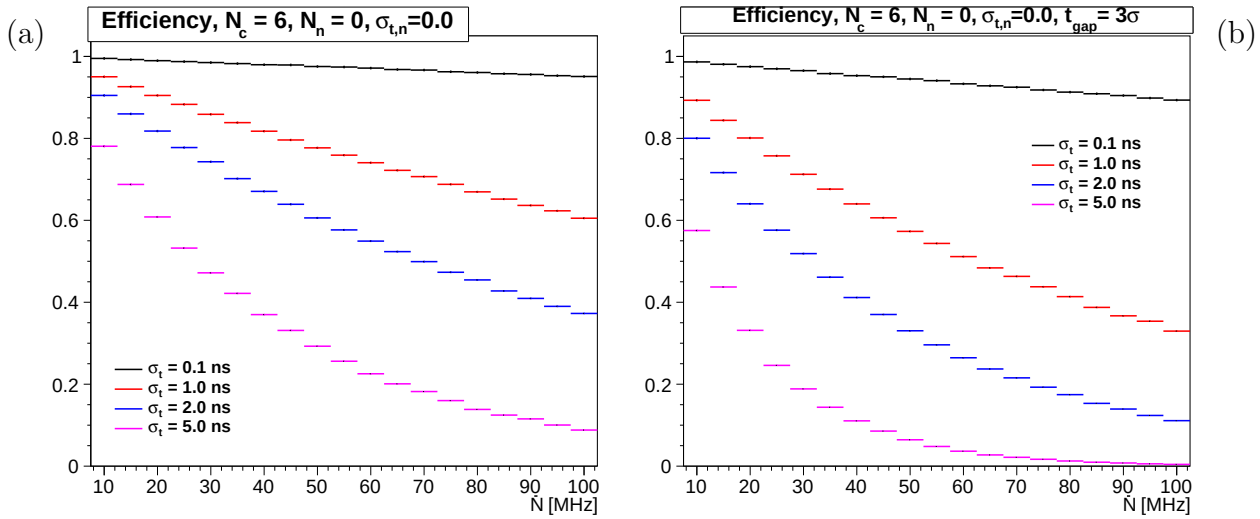

Figure 3: Event rate dependent efficiency based on pure overlap (a) and on an event building algorithm (b) described in the text for reactions with $N_c = 6$ charged tracks. The values are plotted for instantaneous rates between 10 MHz and 100 MHz and time resolutions of $\sigma_t \in \{0.1, 1.0, 2.0, 5.0\}$ ns, colored in black, red, blue and magenta, respectively.

differences δt larger than a certain value t_{gap}. The gap has been set to $t_{\text{gap}} = 3\sigma_t$ for the current investigation. The corresponding results for that method are shown in fig. 3 (b). Obviously all the efficiencies drop compared to the corresponding non-overlap fractions shown in fig. 3 (a) as expected since those represent upper limits of realistic efficiency values. Nevertheless the advantage is still highly significant for $\sigma_t = 0.1$ ns which still shows values of $\epsilon(100\text{ MHz}) \approx 90\%$, where in the other cases the efficiency loss at high rates is much more prominent.

However, the key issue are not the efficiencies for the instantaneous rates, but the time-averaged

σ_t [ns]	0.1	1.0	2.0	5.0
$\overline{\epsilon}$(50MHz)[%]	97	75	58	29
$\overline{\epsilon}$(100MHz)[%]	94	58	36	12
$G_{0.1}$(50MHz))	-	1.3	1.7	3.3
$G_{0.1}$(100MHz))	-	1.7	2.6	7.8

Table 2: The first two rows contain the time weighted efficiencies for the two different peak rates and four different track time resolutions. The last two rows shown the relative gain factor of the efficiencies to the scenario with $\sigma_t = 0.1$ ns.

efficiency

$$\overline{\epsilon} = \frac{1}{N} \int_0^{t\text{run}} \dot{N}(t) \cdot \epsilon(\dot{N}(t))\, dt \quad , \quad N = \int_0^{t\text{run}} \dot{N}(t)\, dt$$

with N being the total number of reactions taking place within time t_{run}. The value $\overline{\epsilon}$ represents the fraction of reactions during a longer period of data taking, which can be selected solely based on timing. For that purpose a time dependent event rate of the form

$$\dot{N}(t) = a_0 \cdot \exp(-a_1 \cdot t) + a_2$$

has been modeled to imitate the behaviour of the beam current with the properties of having a peak rate of 50 MHz [5] and an time average rate of 20 MHz corresponding to PANDA's high luminosity mode.

These values $\overline{\epsilon}$ have been determined for maximum event rates of 50 MHz and 100 MHz to take into account both the cluster jet and pellet target option. The same four time resolutions as previously given have been studied: $\sigma_t \in \{0.1, 1.0, 2.0, 5.0\}$ ns.

The results of the weighted intergrals are shown in tab. 2. The first two rows contain the values for all combinations of rates and time resolutions. In order to explicitely quantify the gain of having a precise timing detector, the last two rows show the relativ factors

$$G_{0.1}(\overline{\epsilon}) := \frac{\overline{\epsilon}(0.1 \text{ ns})}{\overline{\epsilon}}$$

which effectively expresses how many more events can be properly reconstructed using a simple event building algorithm.

The minimal improvement of having a time resolution of $\sigma_t = 0.1$ ns instead of $\sigma_t = 1$ ns is 30% ($G_{0.1} = 1.3$) for peak event rates of 50 MHz. The maximum gain factor $G_{0.1} = 7.8$ could be achieved when compared to a time resolution of $\sigma_t = 5$ ns at peak rate 100 MHz, i. e. a high precision time resolution would result in roughly eight times more properly reconstructed events!

Finally it shall be emphasized, that only reactions with charged final states have been taken into account for the considerations at this point. Adding neutral particles to the event building

[5] The case of $\dot{N} = 100$ MHz with the pellet target option is related to the fact that half of the time no reactions take place and the other half of the time the rate has to be twice as high to compensate that. Therefore this case is treated by integrating the same function weighted with the efficiencies $\epsilon(2 \cdot \dot{N})$.

complicates the process, since it is unclear how an algorithm combining particles with different time resolutions should look like.

However, it shall be stressed as well that from the reconstruction point of view a technically simple manageable time-of-flight detector will deliver a good time signal without unpredictable challenges, whereas more complicated devices will need more complex procedures. In particular for online trigger and event building issues a simple timing device would be of major advantage.

3.2 Relative Time of Flight

Due to material constraints PANDA will not have a start detector for Time-of-Flight measurements. This would have to be installed close to the interaction point and all available techniques would introduce too much material affecting track resolution and causing photon conversions.

Nevertheless using Time-of-Flight for particle identification is possible easily in cases where more than one track can be measured. The algorithms for this method of relative Time-of-Flight have been described previously [2]. The method is well established and was previously used in the HADES experiment.

One important additional consideration for PANDA is the fact that in the present baseline setup charged particle identification in the forward spectrometer is performed exclusively by Time-of-Flight. The proposed RICH detector is only an option, which is not yet funded and the forward straw trackers presently do not foresee a measurement of energy loss. There is a class of events in several physics channels where only one charged particle reaches the forward spectrometer which has to be identified to select the signal correctly.

In this case a time input from another charged track detected in the target spectrometer is required to allow relative Time-of-Flight for this forward going charged track. The resolution of the Time-of-Flight measurement for these particles is determined by the resolution of the forward Time-of-Flight detector and the reference timing detector in the target spectrometer. They should therefore be of similar quality. The fraction of these events varies depending on the physics channel between few percent and up to 36% for the channel $\Omega_c\bar{\Omega}_c$ which is just below the maximum CM energy available at HESR. Table 3 displays some important channels with a higher fraction of single forward going charged particles.

Channel	**Beam momentum (GeV/c)**	**Single forward event fraction**
$\Omega_c^0\bar{\Omega}_c^0$	15	36%
$D^{\star+}D^{\star-}$	4.1	18%
$\eta_{c1}\eta$	5.5	17%
$\Omega^-\bar{\Omega}^+$	5.7	16%
$\Lambda_c^+\bar{\Lambda}_c^-$	11.15	15%
$D_s(2317)D_s^-$	4.3	12%

Table 3: Some physics channels simultated by `EvtGen` with a single forward going charged track to be identified by relative ToF.

3.3 Pattern Recognition

A detector with good time resolution outside the central tracker (CT) may serve as a seed for track finding in the CT. This would work best if the detector would resolve both ϕ and z at a reasonable granularity. With this, combinatorics of track hypotheses in the process of pattern recognition could be reduced. This holds for both considered types of central trackers, the STT and the TPC.

In contrast, developing track seeds from the side of the MVD requires more processing time due to the more complicated structure of the MVD and the higher track density. Moreover tracks emerging from weak decays will be missed and require a second pattern recognition pass. Another drawback here is the fact that due to the limited number of layers in the MVD many ghost tracks can be formed confusing the further steps into the CT region. By starting the pattern recognition of the CT at the outside on the contrary, these tracks could serve as seeds for the MVD or at least clean up ghost tracks in the MVD.

Neverthless the benefits of track seeds from a high granularity timing detector would be significantly different for the two CT cases:

- In case of the straw tube tracker (STT) a 2D track seed by a timing detector can simply provide the starting point for the pattern recognition speeding up the process notably without being a fundamental ingredient. It also adds to 3D pattern recognition of the STT providing a starting point in z-direction.

- In the case of the time projection chamber (TPC) the tracks have the uncertainty of the starting time since they drift with t in z-direction. A 2D timing detector with segmentation in z would identify starting time of the tracks drifting within the TPC in a very easily available way allowing faster pattern recognition and more important solve the problem of event association of TPC data to the underlying interactions. No separate algorithms to find tracks from decay vertices within the TPC would be needed.

  Furthermore a very quickly available signal from a 2D timing detector can be inserted into the data processing stream of the TPC already at the frontend level simplifying the electronics, algorithms and requirements on computing power and buffer memory.

The track seeding by the timing detector does not require the highest possible time resolution. But a key issue is to have the hits of the timing detector easily available without further parallel processing or calibration, since otherwise the tracking process would have to wait for this preprocessing. For this reason the EMC is not well suited as a detector for track seeds. In addition it confuses charged and neutral particles.

3.4 Conversion Detection and Charge Discrimination

A fast detector sensitive to charged particles in front of the EMC can serve to detect photon conversions happening inside the other detectors. A layout in which the timing barrel is placed outside the DIRC and immediately in front of the EMC allows the detection of conversions in the

DIRC, which are fairly frequent due to the thickness of the DIRC radiator. If the timing detector in addition has a reasonable spatial resolution a reliable detection and potentially correction of the effect of photon conversions becomes possible.

In a study [5] for the BaBar experiment it was shown that by detecting conversions in the DIRC radiator the resolution for π^0 could be improved by about 5%. Comparing directly samples with and without conversions the resolution is worse by about 50% with conversions. The conversion detection efficiency in the BaBar case was only 50% because the light from conversion electrons had to be detected by the DIRC itself. In BaBar the fraction of signal events spoiled by conversions was 13% and could be reduced to 7.4 % by detecting them. In our case a separate detector outside the DIRC would discover conversions with full efficiency. In addition, for photons at shallow angles a higher percentage of conversions is expected. The proper algorithm to actually recover a conversion remains an open question.

In a similar way this detector can serve as input to the EMC to discriminate charged and neutral particles. This is of particular interest in the phase of software triggering when full track information is not yet available but a preselection of specific topologies requires this information. Plastic scintillators mounted in front of electromagnetic or hadronic calorimeters are used for this purpose in many hadron physics experiments.

4 Detector Layout

In this section we present the design for a scintillator tile hodoscope (SciTil) as general purpose timing detector in PANDA.

One of the main concerns with the barrel Time-of-Flight detectors is the influence on the EMC due to its material causing photon conversions. This effect is reduced to a minimum if one places the detector material as close as possible to the EMC and tries to reduce it to the absolute minimum. In case of the scintillator based barrel ToF the main reason for the thickness is the length of the scintillator bars leading to high light attenuation and in turn to the need for a thicker scintillator to still have an acceptable light yield at the photon detector.

Taking all these concerns into account one arrives at a new timing detector concept based on small 5 mm thin plastic scintillator tiles coupled directly to Silicon Photomultipliers (SiPM) with excellent time resolution to read out the scintillation light. A minimum ionizing particle generates approximately 10000 photons across the tile thickness of which about 100 are directly measured by the SiPMs. This allows a threshold well above the intrinsic noise of the SiPMs.

The initial idea foresaw a 1:1 matching with the front faces of the calorimeter crystals to achieve the shortest possible distance. Studies on the impact on the mechanical design of the EMC lead, however, to the conclusion, that the required temperature stability of the crystals to an accuracy of 0.1 K cannot be achieved any more with the insertion of another detector system with sensors and readout electronics. In addition the inclination of the tiles would lead to an increased thickness of the EMC structure leading to displacements of the detectors inside the EMC. Another disadvantage of this inclination is that at larger angles gaps open up reducing the geometrical acceptance for decay particles.

Therefore it was decided to insert the SciTil arranged as a flat barrel into the volume foreseen for DIRC and TOF. In this way the minimal thickness can be achieved and the EMC crystals are not disturbed. In addition backsplash from the calorimeter into the scintillator in this configuration is not a big issue any more. While initially the scintillator tile size was determined by the crystal front face of 2×2 cm^2 a slightly increased size of approx. 3×3 cm^2 is suitable as well reducing the number of readout channels.

The advantages of the concept are as follows: The concept results in the lowest possible material budget. It provides fast timing in the order of 100 ps for a flexible software trigger and Time-of-Flight. Placing it just at the outside of the DIRC bars it allows clean detection of γ-conversions in front of the EMC in particular within the close by DIRC. In addition it is well suited for charged-neutral discrimination. Furthermore an endcap SciTil detector could essentially be built from the same building blocks as the barrel detector providing precise timing where it was previously missing altogether. This detector provides space resolved timing signals as input to trigger matrices and track finding.

In the following subsections details of the design of the barrel SciTil detector are given.

4.1 Mechanics

The basic unit of the SciTil detector is the scintillator tile to which two SiPMs are attached on different sides to allow the collection of photons from all locations within the scintillator volume. The size of the tile is given by the placement just outside the DIRC bars and is in the presented layout 28.5 mm in width and length and 5 mm in thickness. This basic building block is depicted in Fig. 4.

Four tiles are arranged with their SiPMs in one module in a way that they all point to the inside of the unit to minimize acceptance losses as can be seen in Fig. 5 a). The four tiles are read out by one readout card containing an 8-channel readout ASIC and a protocol chip for arbitrated data transfer on differential serial links to reduce the amount of cables. The complete quad tile module is shown in Fig. 5 b).

On top of one DIRC bar box one SciTil box is placed with 30 quad modules in z-direction and 3 quad modules in azimuthal direction totalling 360 tiles. The acceptance region in PANDA coordinates is from z=-500 mm till z=1500 mm matching the angular coverage of the DIRC and the Central Tracker. The radial thickness of a SciTil super-module is 1.8 cm. One such SciTil super-module is shown in Fig. 6. Cooling of each super-module is done by means of cooled air flow. The entire half barrel of the SciTil detector composed of 8 super-modules is represented in Fig. 7.

The layout of the SciTil detector is done in close conncection with the mechanical design of the DIRC detector. It fits in the available space and has no impact on the EMC nor on the Central Tracker concerning dimensions. All dimensions and numbers of elements are given in table 4.

Element	**Dimensions**	**per Module**	**per Super-Module**	**Total**
Scintillator Tile	$28.5 \times 28.5 \times 5$ mm^3	4	360	5760
SiPM	$3.85 \times 4.3 \times 1.45$ mm^3 (3×3 mm^2 active)	8	720	11520
Module	$60 \times 60 \times 12$ mm^3	1	90	1440
Super-Module	$180 \times 1800 \times 18$ mm^3	na	1	16

Table 4: Table of properties of the Barrel SciTil detector.

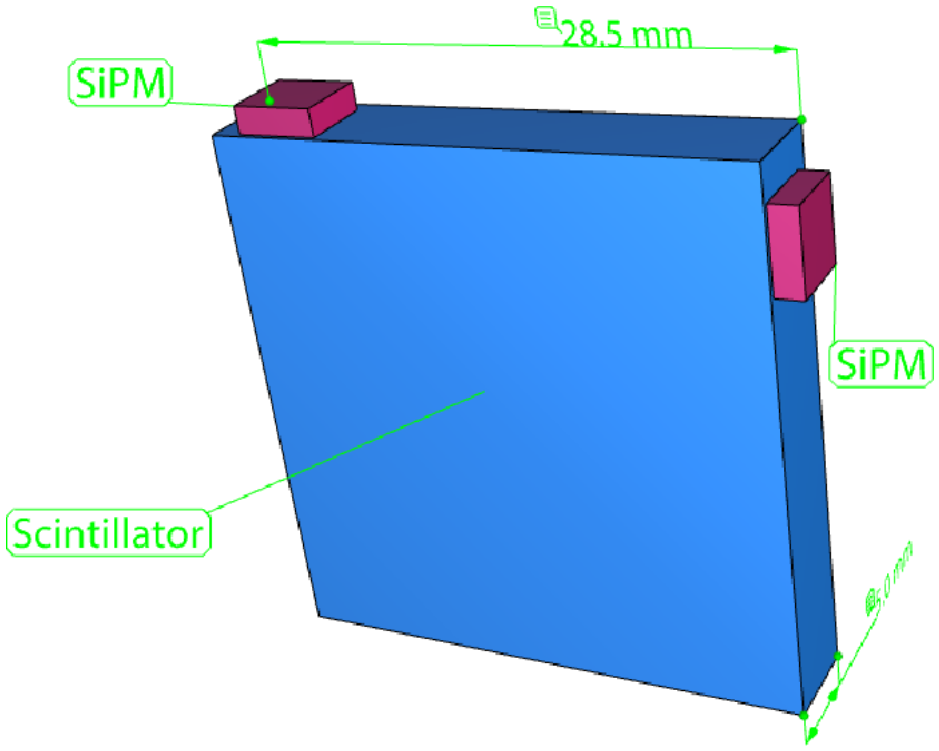

Figure 4: A single scintillator tile with SiPMs attached.

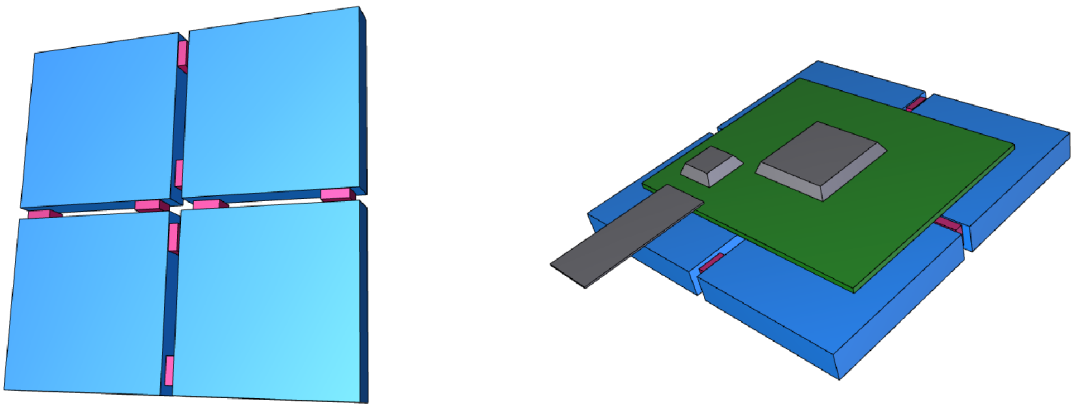

a) b)

Figure 5: a) Four tiles arranged with their SiPMs for densest packing. b) A quad tile module with a readout PCB containing one 8-channel readout ASIC and a data transfer chip.

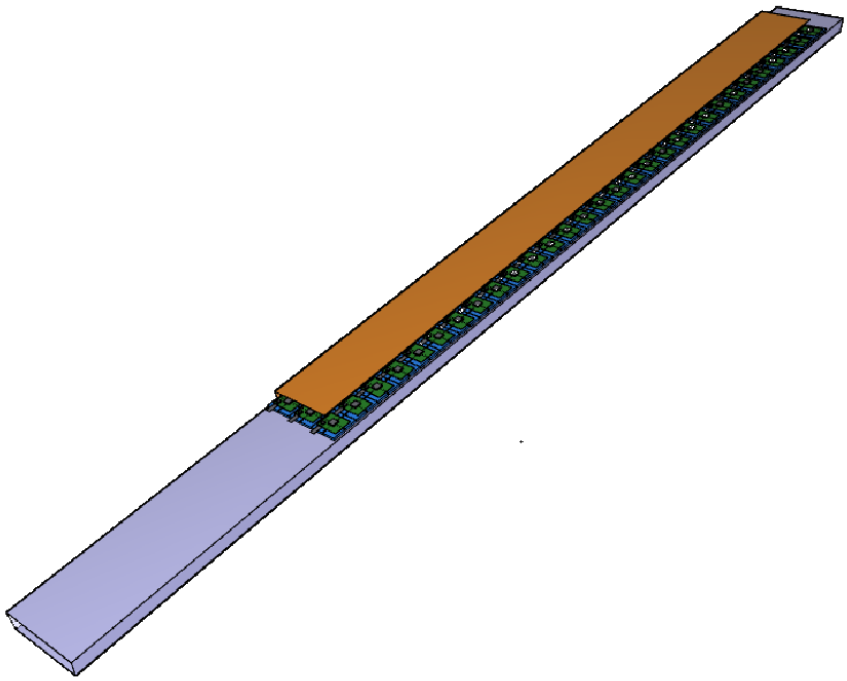

Figure 6: A SciTil super-module composed of 90 quad modules shown on top of a DIRC bar box.

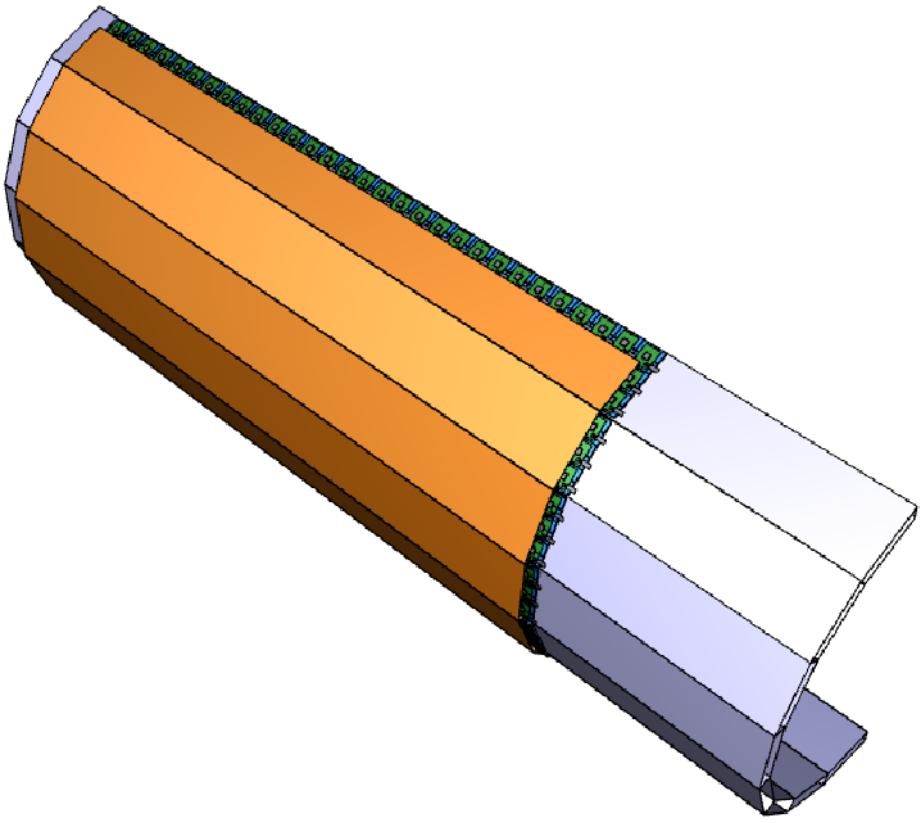

Figure 7: An entire SciTil half barrel composed of 8 super-modules.

4.2 Scintillator

Scintillators for fast timing applications need short decay times and plenty of photons. The many photons serve for clean trigger conditions, the timing itself is done with the first arriving photon. The decay of excited levels occurs exponentially in time. Thus, the time difference between excitation and emission of the first photon is inversely proportional to the number of photons and proportional to the decay time. There is also the risetime of the signal involved. The rise time depends on the energy transfer mechanism within the scintillator [12]. If the rise time reaches values comparable to the decay time of the scintillator material, the time resolution as function of the number N of photons changes its behavior. It goes from $\sigma = \sigma_0/N$ to a $\sigma = \sigma_0/\sqrt{N}$ dependency. This is experimentally known for a long time [10].

A simple simulation shows the influence of the risetime. In Fig. 8 the RMS of the first emitted photon is shown for many events as function of the number of photons in a single event. The curves are for different assumptions of the photon emission probability (signal lineshape). The values chosen are for a BC-408 scintillator [11] which has a risetime of $\tau_R = 0.9\,\text{ns}$ and a decaytime

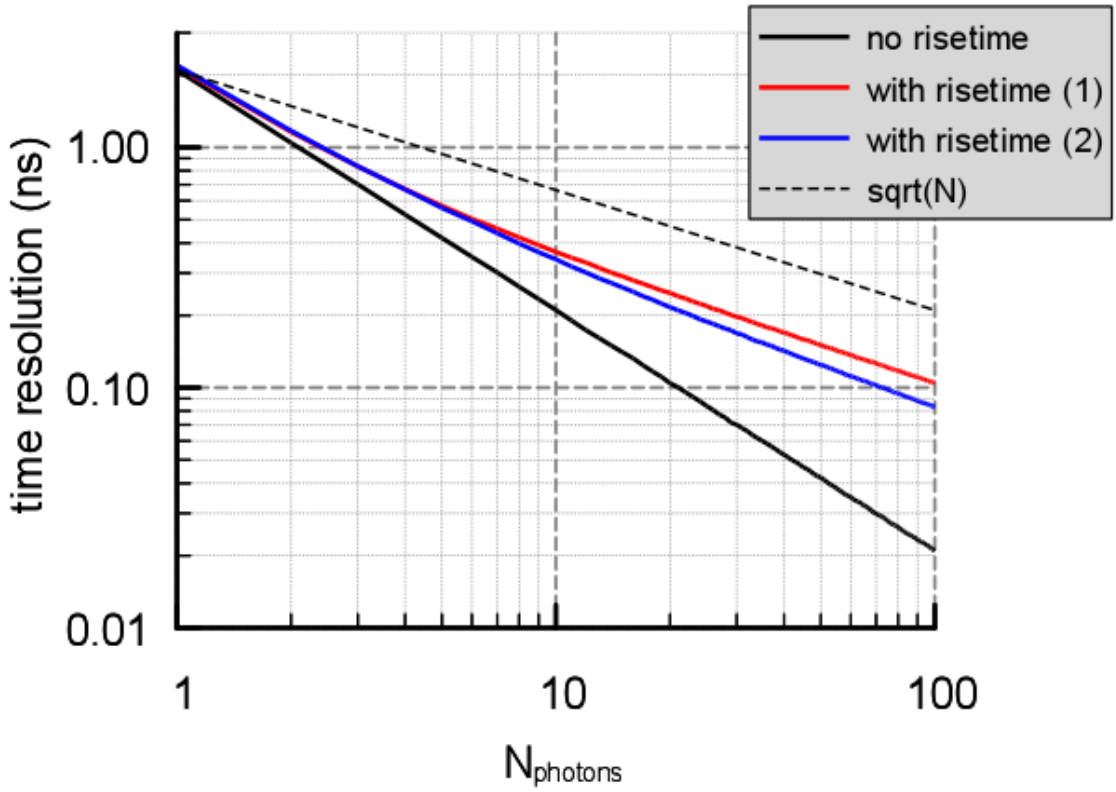

Figure 8: Simulation of the time resolution of BC-408 scintillator [11] depending on the number of measured photons. The black curve is the achievable time resolution (RMS) for an pure exponential photon emission in time with $\tau_D = 2.1\,\text{ns}$. The red curve is for an additional smearing of the decay time with an Gaussian of width $\sigma = 0.9\,\text{ns}$ leading to a risetime. The blue one is for a different decay shape of $(1 - \exp(-t/\tau_R))\exp(-t/\tau_D)$, with $\tau_D = 2.1\,\text{ns}$ and $\tau_R = 0.9\,\text{ns}$.

of $\tau_D = 2.1\,\text{ns}$. The black curve is for a pure exponential decay and follows $\sigma = \sigma_0/N$. For the risetime two assumptions for the lineshape were made. The red curve is for an exponential decay whose start was smeared with a Gaussian distribution with $\sigma = \tau_R$, the blue curve is for an exponential risetime followed by an exponential decay sampled by $(1 - \exp(-t/\tau_R))\exp(-t/\tau_D)$. Both assumptions produce similar results and follow a $\sigma = \sigma_0/\sqrt{N}$ dependency shown by the dashed line. When photons are lost due to geometry or quantum efficiency of the photon detector, the number of measured photons has to be taken for this consideration.

Scintillation Properties –	**BC-400**	**BC-404**	**BC-408**	**BC-412**	**BC-416**
Light Output, %Anthracene	65	68	64	60	38
Rise Time, ns	0.9	0.7	0.9	1.0	–
Decay Time (ns)	2.4	1.8	2.1	3.3	4.0
Pulse Width, FWHM, ns	2.7	2.2	~2.5	4.2	5.3
Wavelength of Max. Emission, nm	423	408	425	434	434
Light Attenuation Length, cm*	160	140	210	210	210
Bulk Light Attenuation Length, cm	250	160	380	400	400

Scintillation Properties –	**BC-418**	**BC-420**	**BC-422**
Light Output, % Anthracene	67	64	55
Rise Time, ns	0.5	0.5	0.35
Decay Time, ns	1.4	1.5	1.6
Pulse Width, FWHM, ns	1.2	1.3	1.3
Wavelength of Max. Emission, nm	391	391	370
Light Attenuation Length, cm*	NA**	140	NA**
Bulk Light Attenuation Length, cm	100	110	8

Table 5: Physical properties of organic plastic scintillators from Saint-Gobain-Crystals (former BICRON) [11]

In order to achieve a time resolution of $\approx 100\,\text{ps}$ one needs a sufficient number of photons to decrease the time jitter σ_j of a single photon to $\sigma_{j,N} = \sigma_g/\sqrt{N}$ [10]. The time jitter for the measured single photon depends on the possible light paths within the scintillator, the detection device, and the readout chain. If the latter two have an acceptable performance, the geometry of the scintillator has to be chosen such that the light path variations from the scintillation towards the photon detector are small. For a time resolution of $\sigma \approx 100\,\text{ps}$ and the effective speed of light

within e.g. BC-408 scintillator of $c_{scint.} \approx 150\,\mathrm{mm/ns}$ [16] scintillator tiles of 20-30 mm should be chosen read out from two sides. It is known that the effective speed of light in a scintillator is slower than the nominal one, calculated from the refractive index [12, 16, 17, 18].

The physical properties of organic plastic scintillators [11] are shown in Table 5. Scintillators which are used for time of flight detectors are usually BC-404 and BC-408. For long scintillators in the order of 1 m the bulk attenuation becomes an issue. These scintillators need a certain thickness of several cm in order to produce a sufficient number of photons which reach the photon detector without absorption. For small sized geometries with $\approx 5\,\mathrm{mm}$ thick scintillators this requirement is less stringent and the scintillator BC-420 might be an option. An example for 2300 mm long and 50 mm thick BC-408 scintillators is the TOF-barrel of the BESIII at BEPCII experiment [13]. Here, a time resolution of $\sigma = 80 - 100\,\mathrm{ps}$ has been achieved. Another example with 200 mm long and 8 mm thick BC-404 scintillators is the PHOBOS detector at RHIC. The measured time resolution is $\sigma = 75\,\mathrm{ps}$ [14]. Both detector systems use photomultiplier tubes for photon detection.

For a $30 \times 30 \times 5\,\mathrm{mm}^3$ scintillator tile the expected measured photon number is calculated as follows: A minimum ionizing particle with an energy loss of 1 MeV in the 5mm thick scintillator generates 10000 photons, assuming that a photon needs 100 eV energy [15]. The fraction of 30%

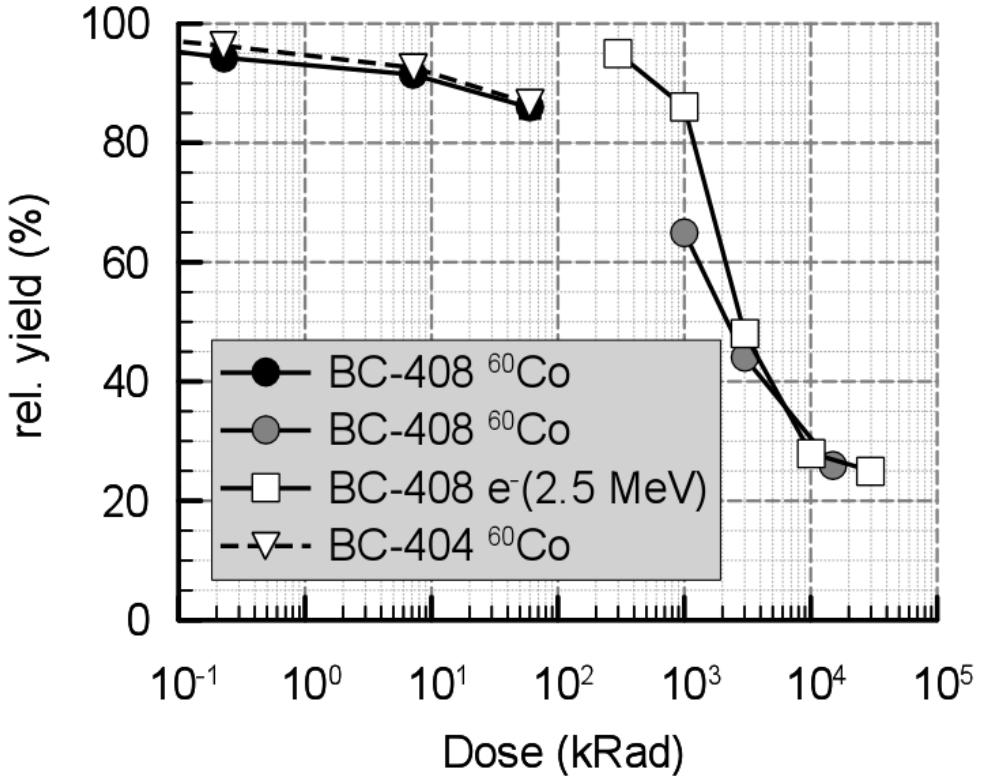

Figure 9: Relative light yield of BC-404 and BC-408 scintillators irradiated with gammas from ^{60}Co and electrons with energies of 2.5 MeV. Black circles and white triangles from [19], gray circles from [21], white squares from [20]

of the isotropic directed photons leave the scintillator through the large surfaces and a fraction of 70% is reflected towards the rim with an area of 600 mm^2. Therefore the rim is hit by 12 mm^{-2} photons. Covering the rim with two photon sensors with a total area of 18 mm^2 and a photon detection efficiency of 55% (Chap. 4.3) yield 120 measured photons. For a $20 \times 20 \times 5\,mm^3$ tile this number increases to 180 measured photons.

The high interaction rate of the PANDA experiment requires a radiation hardness of the scintillator. The values of relative light yield of two scintillators BC-408 and BC-404 after different levels of irradiation are shown in Fig. 9. The black circles and white triangles are from Li et al. [19] and show results of an irradiation of BC-404 and BC-408 using a ^{60}Co source, the gray circles from Zorn et al. [21] are for BC-408 at higher radiation doses, and the white squares from Majewski et al. [20] represent irradiation of BC-408 with 2.5 MeV electrons. It is obvious that these scintillators withstand radiation doses of 100 to 1000 kRad having more than 80% of relative light yield. For the irradiation with electrons of 2.5 MeV energy [20] the light yield drops to 48% at 3 MRad accumulated radiation. After a recovery time of 20 days the light yield of the BC-408 scintillator reached values between 80% and 90%. Such recovery is not observed for gammas [19].

4.3 Photon Detector

A Geiger-mode avalanche photo diode sensor matrix, the so-called SiPM, will be used to detect the scintillation light originating in the plastic scintillator tiles after transition of a charged particle. The SiPM is now readily available on the solid state photon sensor market and is produced by various companies. This sensor is based on single avalanche photodiodes (SPAD), a digital sensor for the occurrence of a photon, by combining a large number of SPAD-cells in parallel. Thus a digital photon sensor becomes a quasi-linear device if the number of simultaneous photons in the matrix is much smaller than the number of active micro cells. This idea was first followed up in Russia by V.Golovin [28] and Z. Sadygov [29] and the first sensors have been produced there by standard MOS techniques. A comprehensive overview including the historical roots and the present state of development of the SiPM can be found in the paper by Renker and Lorenz [30]. The application of SiPM in physics is still quite new, however, examples of larger scale applications in calorimetry like Calice [32] or T2K [31] and timing like MuSR[33] have already been very successful. Here we refer also to EU projects in HadronPhysics2 in which the development of SiPM together with new detector systems is proposed [34] (HP2) and in HadronPhysics3, where the development of the SciTil is one of the R&D topics [35].

SiPMs have a very good photon detection efficiency (PDE) with single photon resolution, excellent timing properties and operate in high magnetic fields. They have high gain and high rate capability. In contrast to photomultipliers they are very small, robust and need only low bias voltage. Drawbacks may arise from relatively high single photo-electron noise and the sensitivity to temperature variations due to silicon being the active material. In practice, the crosstalk between the micro cells as well as the single cell recovery time may be an important parameter.

At present SiPM sensor matrices are available with only small active area. The 3×3 mm^2 area sensor is the most common type differing mainly in the density of micro cells of 10^2 to $4 \cdot 10^4$ cells/mm^2. For larger active area matrices of up to 8×8 SiPM are being offered by a few companies.

Selection criteria of the SiPM for the Scintillating Tile Hodoscope. We consider here four sensors from four different producers, namely Hamamatsu, Zectotek, KETEK, and AdvansID (FBK-Irst). A summary of parameters relevant for the application on the scintillating tiles is shown in Tab. 6.

Signal rise time: SiPMs are intrinsically very fast devices since the avalanche region is very

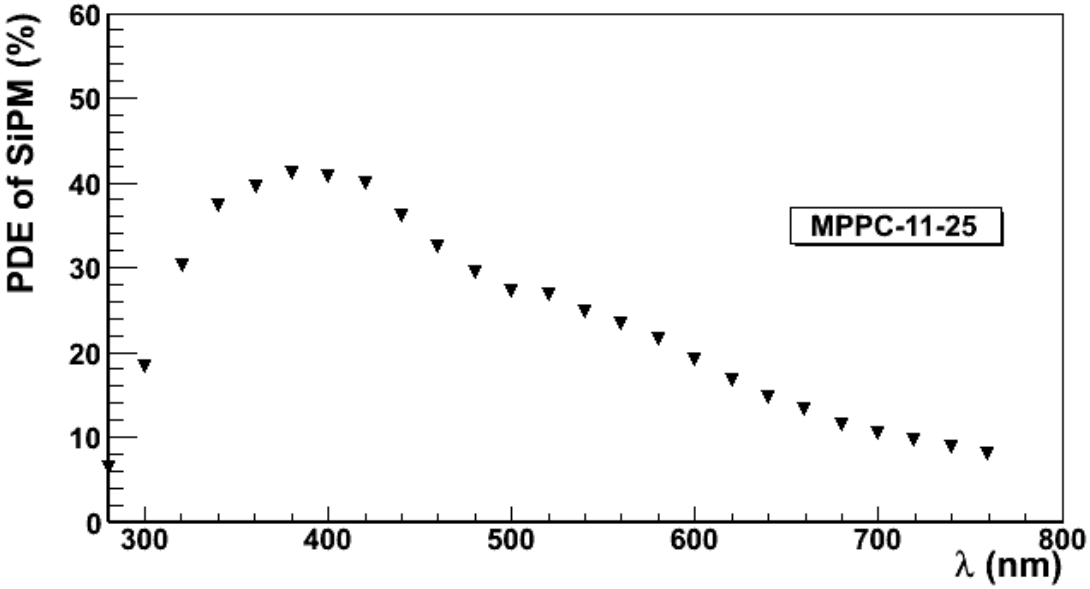

Figure 10: Photon detection efficiency of the Hamamatsu sensor from the S 10362-11 series with 400 pixels/mm^2.

SiPM	Micro cell size μ	Micro cells /mm^2	Bias voltage V	PDE at λ=430 nm	Gain	Dark Rate Mcps at 0.5 p.e.	Signal rise time ns	Material
Hamamatsu S10931-100P	100	100	72	55	7x10^5	7	< 1	P on N
Zecotek MAPD3N	8	15000	90	30	5x10^4	8	< 2	P on N
KETEK 50D2	50	400	30	40	5x10^5	10	< 1	P on N
AdvansID (FBK-irst)	40	400	30	15	1.5x10^6	18	< 1	N on P

Table 6: Characteristics of sensors from different vendors.

thin (1-3 μm). Thus the transit time spread is very small and the rise time of the signal very much depends on coupling to the following preamplifier which should have a low input impedance. Subsequently, it will be the bandwidth of electronics determining the signal rise time.

Signal decay time: Depending on the producer typical values for the signal decay time are from 5 ns to 50 ns. This number reflects the interior processes during the avalanche and can probably improved in future production processes.

Photon detection efficiency (PDE):

$$PDE = QE \cdot \epsilon \cdot P(trigger)$$

The quantum efficiency determines the spectral sensitivity. It is around 80 percent at $\lambda = 400$ nm. The epoxy surface layer starts to cut off at shorter wave length. Hence, working with unprotected sensors may be possible to enhance QE at the maximum of the emission spectrum of the scintillator. So matching to the emission spectrum of the scintillator to the spectral sensitivity is an important criterion. The probability of triggering an avalanche after absorption of a photon is typically higher than 80 percent. The geometric factor ϵ depends very much on cell size as well as the techniques of putting isolating trenches in between. For the surface type sensors (Hamamatsu e.g.) with isolated 100 μm size cells, ϵ can be up to 90 percent. However, for better linearity a 50 μm cell size might be preferable for the SciTil. A typical PDE for Hamamatsu and Zecotek sensor is shown in Fig. 10 and Fig. 11.

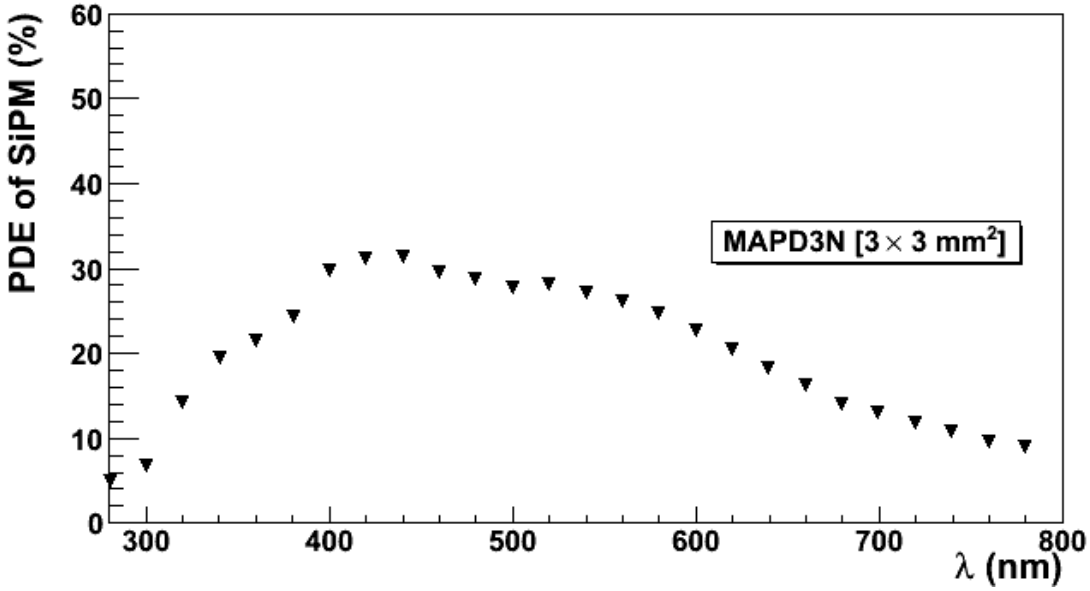

Figure 11: Photon detection efficiency of the Zecotek sensor from the MAPD3N series with 15000 pixels/mm^2.

Signal linearity: This property is less important for the SciTil. The photon collection efficiency in a tile depends on the geometric position on the tile of the impinging charged particle, which entails very different signal amplitudes .

Gain: The absolute gain is not a serious issue as long as it stays above 5×10^4. However the gain stability matters. Therefore a temperature control of $\pm 1°C$ should be maintained.

Noise: The SiPM is intrinsically a noisy device with up to 1 MHz pulse rate per mm^2 sensor surface ($T = 20°C$) at the single photo-electron amplitude. It becomes negligible at trigger levels of 10 photons and higher. The timing is not effected since the output signal contains the first photons as well. This noise may be reduced by a factor of ten when working 30°C lower, which is not considered here.

Radiation Hardness: There have been various studies on radiation effects in SiPM. In general, the surface type sensors exhibit deterioration of gain and increase in noise behavior. The MAPD3N from Zecotek, where the pixels are lithographically embedded below the avalanche region, the so-called micro-wells, are less effected by radiation. A dose as it is expected for the SciTil in PANDA may be compatible. A special radiation hard type is under development.

Housing: An important consideration can be the housing of the sensor. It has to be flat with a flat sensor surface to be able to glue it to the the scintillator. Since we need a large number, the manufacturing process of the housing should be fully automated including the bonding to the quenching resistor. Thus the price for a sensor unit might come down to below 10 Euro per piece.

In summary, the SiPM is an ideal photo sensor for the SciTil. It behaves like a miniature photo tube the output signal being unaffected by a 2 Tesla magnetic field. It can be mounted together with preamplifier and integrated electronics directly to the scintillator tile. If we had to choose the SiPM today the device from Hamamatsu would have our preference due to the higher PDE compared to others. It remains to be seen how the development of the digital SiPM advances in which sensor and readout electronics are combined on the same chip, and the intrinsically digital information from the sensor is digitally transferred to the DAQ.

4.4 Electronics

As shown in Fig. 5 b) the present layout for the SciTil detector foresees modules composed of four scintillator tiles with two SiPMs each which are read out by one 8-channel ASIC mounted on a PCB together with a chip for data transmission.

The readout ASIC is supposed to amplify and discriminate the SiPM signal in a way that the very good intrinsic time resolution of the SiPM is maintained. After discrimination a precision time stamp should be generated for each valid hit. This can be achieved by implementing a TDC on the ASIC or building blocks like voltage controlled oscillators or delay locked loops. The output is a digital differential signal.

As the second major component a data transmission chip serializes the input of the board's ASIC and merges it into a passing through serial data stream. In this way individual cables from each

module to the readout concentrators can be avoided but are cascaded in z along the whole barrel length. If this chip can be an FPGA using special programming to protect from single event upset by radiation or if it has to be as well an ASIC still has to be determined.

In table 7 a number of existing SiPM readout ASICs are summarized. This review was done by W. Kucewicz at the occasion of a Industry-academia matching event on SiPM and related technologies at CERN on February 16 and 17 2011 [23].

Chip Name	**Channels**	**Time Resolution**	**Technology**	**Reference**
SPIROC	36	100 ps	0.35 μm SiGe	[24]
PETA	40	50 ps	0.18 μm CMOS	[25]
BASIC	8/32	120 ps	0.35 μm CMOS	[26]

Table 7: Summary of existing SiPM readout ASICs which digitize charge and time [23].

The ASIC to use in the SciTil detector does not necessarily have to digitize the pulse charge since the high precision time of a valid hit is the basic required information. Nevertheless understanding noise and aging profits from a charge readout. However the most stringent requirement is the optimized time resolution of the chip.

If a modified version of an existing chip will be employed or a new chip will be developed depends also on the outcome of the cooperation on SiPMs and their readout within the framework of the European Initiative on Hadron Physics (I3HP3) [35]. Power consumption and time resolution are the key parameters in the final decision on the readout.

Finally, a conceptionally different alternative is the digital SiPM developed by Philips. Here low-power CMOS electronics is integrated directly into the SiPM chip. Each firing SiPM cell is counted and the detection of the first photon creates a signal timestamp. In this way the SiPM becomes a fully digital device which can be connected directly to higher level readout electronics avoiding power consuming analog amplification and digitization [27].

5 Organization

5.1 Cost Estimate

Based on first quotations from industry and prior experience for similar components a first rough cost estimate was derived. This is presented in table 8. It quotes both the cost for the barrel part of the SciTil as well as for the endcap part. However mechanical details of the endcap part are not yet as advanced as for the barrel part.

Element	**Unit cost** (EUR)	**Barrel** (kEUR)	**Endcap** (kEUR)	**Total** (kEUR)
Scintillator Tiles	25	140	50	190
SiPM	30	330	120	450
Readout	20	220	80	300
Mechanics		50	20	70
Sum		740	270	1010

Table 8: Table of cost of the SciTil detector.

5.2 Project Structure

The project awaits the general approval of the $\overline{\text{P}}$ANDA collaboration for a timing detector as well as for this specific types. Table 9 represents the current status of work share and interests. However funding still has to be applied for and further groups are welcome to strengthen the efforts for the SciTil detector. The interested groups are Bhabba Atomic Research Center Mumbai (India), JINR Dubna (Russia), INPI Gatchina (Russia), and GSI Darmstadt (Germany) with its involvement in the activity on SiPMs with in the EU I3 Hadron Physics.

The work packages of the SciTil project are briefly explained in the following:

Simulation: The optimal arrangement and number of photon sensors on the scintillator will be evaluated. The geometrical acceptance has to be optimized.

Module design: The simulation results will be verified in module tests with scintillators and SiPMs. Further design issues are the placement of readout electronics.

Scintillator development: Presently industry is well able to provide scintillator elements of suitable size, finishing and quality. Nevertheless an alternative in-house production of scintillator tiles in Dubna may be investigated.

SiPM development, testing and characterization: Different types of SiPMs have to be tested and the time response has to be optimized. Components presently available on the market will be tested in various institutes.

On the other hand the possibility of a SiPM development in India is explored in parallel. In this connection, R&D work related to the device simulation of SiPM and testing of SiPM

are being carried out at BARC by different groups. Involvement of foundries like BEL (Bharat Electronics Ltd.), Bangalore, India can be foreseen for the manufacturing of silicon photomultipliers.

A further interest is the pursuit of the development of more radiation hard SiPMs based on deep microwell structures in Dubna.

Concerning the examination of the radiation hardness of SiPMs the possibility of beam tests in Gatchina are examined.

SiPM readout (ASIC) design: A crucial component is the readout electronics attached to the SiPMs. Here the view is to implement an ASIC with a preamplifier and discriminator and potentially also a TDC mounted close to the SiPM.

Several possibilities are pursued in this context:

- The modification of an existing chip would be a simple solution, provided such a suitable ASIC exists. A market survey followed by tests of samples will clarify the validity of this option.
- The possibility of a development of ASIC electronics with the involvement of the Electronics Division (ED), BARC is investigated.
- Within the framework of the European Infrastructure Initiative I3HP3 collaboration on the development of an ASIC suited for the digitization of SiPM signals is planned.

Mechanical design: Since the detector system will be mounted in close distance to the DIRC quartz bars a close collaboration with the DIRC group of PANDA is required which will be coordinated and guided by the GSI group.

Prototype production: After single unit test and fixing the various design issues, the goal will be to construct a prototype hodoscope to integrate with the prototype DIRC sub-module.

Work package	**Interested institutes**
Simulation	BARC
Module design	GSI, BARC
Scintillator	Dubna, Gatchina
Silicon PM	EU HP3, BARC, Dubna, Gatchina
Readout design	EU HP3, BARC
Mechanical design	GSI
Prototype production	BARC

Table 9: Interests and work share within the SciTil project.

6 Summary

We propose a timing detector for $\overline{\mathsf{P}}$ANDA based on small scintillator tiles read out by silicon photomultipliers. This detector design represents the thinnest possible option for such a detector in $\overline{\mathsf{P}}$ANDA both in terms of material budget and radial dimension.

The motivation for this detector is on one hand the physics addressed by a barrel time-of-flight detector, i.e. contributing to the identification of charged particles at low momentum. In addition to this, physics in the first run is accessible much easier if a scintillator based detector facilitates the calibration and debugging of the other complex systems.

On the other hand there are several technical benefits which combined are as important as the physics arguments. In particular having this easy to operate detector with its high granularity and time resolution as an ingredient in any software trigger for the very first, fast levels of event selection is essential to cope with the very high rates aimed at by $\overline{\mathsf{P}}$ANDA. The detector also serves as inputs for several other detectors: The forward time-of-flight detector can not identify single charged tracks without a reference time. The pattern recognition of the central tracker can profit greatly from a well timed track seed. And finally the EMC profits from the detection of photon conversions and fast charge discrimination.

For this proposal the mechanical design of the SciTil detector was worked out in conjunction with the barrel DIRC to a level of detail which allows the conclusion that there are no mechanical clashes with other detector systems anymore. The components for the systems were discussed and even if SiPMs and their readout electronics presently are a fast evolving field a suitable scenario was presented. Further improvements may still change the final technical design.

With this simple design and the small number of different components a fairly cost-effective detector can be built. The project organisation with its definition of work packages was presented. Several groups have expressed their interest to collaborate on the detector. With the decision to include SciTil into $\overline{\mathsf{P}}$ANDA further strong engagement will be stimulated allowing for a timely completion of the project in spite of its late start.

References

[1] $\overline{\text{P}}$ANDA Collaboration, Technical Progress Report, FAIR-ESAC/Pbar 2005

[2] A. Gillitzer et al., "Motivation of the Barrel Time-of-Flight Detector for PANDA", PANDA Note, January 2011.
http://panda-wiki.gsi.de/cgi-bin/view/Tof/TimingBarrel

[3] G. Schepers et al., "Particle Identification at PANDA - Report of the PID TAG", PANDA Note, March 2009.
http://www-panda.gsi.de/db/notesDBr/GS14-090310_pid-tag.pdf

[4] K. Götzen, "Influence of Particle Timing on Event Building", PANDA Note, March 2011.
http://www-panda.gsi.de/db/notesDBr/KG13-110311_KGoetzen_EventMixingAtPanda.pdf

[5] A. Adametz, "Preshower Measurement with the Cherenkov Detector of the BaBar Experiment", Diploma Thesis, Heidelberg University, January 2005.
http://www.physi.uni-heidelberg.de/Publications/adametz05.pdf

[6] C.J.Batty, E.Friedman, A.Gal, Phys. Rev. C **59**, 295-304(1999).

[7] S. A. Bass et al., Prog. Part. Nucl. Phys. **41**, 225 (1998).

[8] A. Galoyan, Private Comunication.

[9] I. Augustin, H.H. Gutbrod, D. Krämer, K. Langanke, H. Stöcker, Fourth International Conference on Fission and Properties of Neutron-Rich nuclei,Sanibel Island, Florida, 2007; arXiv:0804.0177v1 [hep-ph].

[10] J. Pouthas, S. Agarwal, M. Engrand, and C. Pisani, Nucl. Instr. Meth. 145 (1977) 445.

[11] Saint Gobain Crystals
http://www.detectors.saint-gobain.com/uploadedFiles/SGdetectors/Documents/Product_Data_Shee
404-408-412-416-Data-Sheet.pdf http://www.detectors.saint-gobain.com/uploadedFiles/SGdetectors/
420-422-Data-Sheet.pdf

[12] B. Bengtson and M. Moszynski, Nucl. Instr. Meth. 117 (1974) 227.

[13] BES III
http://arxiv.org/pdf/0911.4960v1

[14] B. Back et al., Nucl. Instr. Meth. A499 (2003) 603.

[15] William R. Leo, "Techniques for Nuclear and Particle Physics Experiments", 2nd edition, 1994, Springer-Verlag.

[16] Zhao Li, Heng Yuekun, Wu Chong, Zhao Xiaojian, High En. Phys. Nucl. Phys. Vol. 30 2006 554.

[17] P. Rossi, E. Polli, M. Albicocco, H. Avakiana et al., Nucl. Instr. Meth. A381 (1996) 32.

[18] J.M. Bennloch, M.V. Castillo, A. Ferrer, J. Fuster, et al., Nucl. Instr. Meth. in Phys. Res. A290 (1990) 327

[19] Zhao Li, Wu Chong, Heng Yuekun, Zhao Xiaojian et al., Nucl. Instr. Meth. A552 (2005) 449

[20] S. Majewski, M. Bowen, C. Zorn, K. Johnson et al., Nucl. Instr. Meth. A281 (1989) 500

[21] C. Zorn, M. Bowen, S. Majewski, J. Walker et al., Nucl. Instr. Meth. A273 (1988) 108

[22] SLitrani http://gentitfx.fr/SLitrani/

[23] W. Kucewicz, "Review of ASIC developments for fast readout electronics", presented at the Industry-academia matching event on SiPM and related technologies, CERN, February 16-17, 2011.
http://indico.cern.ch/contributionDisplay.py?contribId=2&confId=117424

[24] M. Bouchel et al., "SPIROC (SiPM Integrated Read-Out Chip): dedicated very front-end electronics for an ILC prototype hadronic calorimeter with SiPM read-out", prepared for the Topical Workshop on Electronics for Particle Physics 2010 (TWEPP-10), Aachen, Germany, September 20-24, 2010.
http://iopscience.iop.org/1748-0221/6/01/C01098

[25] P. Fischer et al. "Fast Self Triggered Multi Channel Readout ASIC for Time- and Energy Measurement", IEEE TNS Vol. 56, No. 3, p.1153

[26] F. Corsi et al., "ASIC development for SiPM readout", prepared for the Pixel 2008 International Workshop Fermilab, Batavia, IL, U.S.A., 23-26 September 2008
http://iopscience.iop.org/1748-0221/4/03/P03004

[27] Y. Hämisch, "Photon Counting with arrays of Digital SiPM's", presented at the Industry-academia matching event on SiPM and related technologies, CERN, February 16-17, 2011.
http://indico.cern.ch/contributionDisplay.py?contribId=25&confId=117424

[28] V.Golovin, "Avalanche Photodetector", Russian Agency for Patents and Trademarks, Patent No. RU 2142175 (1998)

[29] Z.Sadygov, "Avalancche Detector", Russian Agency for Patents and Trademarks, Patent No. RU 2102820 (1998)

[30] D.Renker, E.Lorenz, "Advances in solid state photon detectors", JINST 4, P04004, (2009)

[31] Y. Kudenko et al., "Status of the T2K experiment", CHEP'06 , Moscow, 2006

[32] I. Laktineh et al. , "Calice, results and future plans", CHEP10, Paris 2010

[33] A. Stoykov et al., "Fast timing detectors for high field MuSR spectrometers", 2008

[34] H.Orth et al, "Matrix Geiger-mode Avalanche Micro-Pixel Photo Diodes for Frontier Detector Systems, in HadronPhysics2", Study of strongly interacting matter, Grant agreement no.: 227431

[35] C. Guaraldo, "HadronPhysics3 Proposal", submitted to EC in Dec. 2010.